PAPER

Check for updates

Influence of surface defects on activity and selectivity: a quantitative study of structure sensitivity of Pd catalysts for acetylene hydrogenation†

Wenbo Xie and P. Hu ![ORCID] *

As one of the essential processes in the energy industry, acetylene hydrogenation reactions have been studied extensively in both experiment and theory. However, the fundamentals of structure sensitivity of acetylene hydrogenation over Pd catalysts are still debatable. Herein, a newly developed coverage-dependent microkinetic modelling is utilized to investigate the structure sensitivity of Pd catalysts. The key reaction kinetics are quantitatively examined; for example, a high ethylene activity of 3.92 s^{-1} and a low selectivity of 0.2 at 300 K are calculated. It is found that the Pd(211) surface is much more active than Pd(111), but exhibits a poor selectivity toward ethylene in contrast to Pd(111) that is intrinsically selective toward ethylene. The high activity of Pd(211) is primarily due to the decisive role of the coverage effect in reducing the reaction barrier of the rate-determining step, while the poor selectivity is a consequence of the inherently high chemisorption energy of ethylene. Furthermore, the ethylene selectivity is found to be more sensitive to the desorption barrier at low temperature. This work provides an atomic-scale understanding of the intrinsic selectivity of the acetylene hydrogenation embodied in different Pd structures.

Introduction

Catalytic hydrogenation is one of the most common reactions in chemical production. It is estimated that 25% of chemical processes involve at least one step of hydrogenation reactions, contributing about 8% of the world GDP, and making it one of the most important areas of catalytic research.[1–3] One of the greatest challenges in hydrogenation reactions is the product selectivity, and hence the understanding, development, and design of efficient and selective hydrogenation catalysts are of paramount importance.[4,5] Ethylene, as a fundamental chemical for industrial usage, is now commonly produced by acetylene selective hydrogenation, which requires not only removing traces of acetylene from ethylene but also avoiding over-hydrogenation leading to the loss of ethylene.[6–8] Generally speaking, acetylene hydrogenation is a tandem reaction in which there are two competing parallel reaction paths: sequential hydrogenation of acetylene to produce ethylene and further hydrogenation to ethane. Also, oligomerization could be a

competitor with the Horiuti–Polanyi mechanism.[9] An ideal catalyst for acetylene hydrogenation should be able to avoid the stepwise hydrogenation of acetylene to ethane.[10,11] Although the emerging non-noble Ni-based[10,12] and Cu-based[13] catalysts are showing convincing potentials, Pd-based catalysts are still the most commonly used catalyst in industries for acetylene hydrogenation and are extensively studied from both experimental[14–17] and theoretical perspectives.[18–23] Interestingly, the activity and selectivity patterns of pure Pd catalysts vary significantly; in some cases, Pd was reported to exhibit considerable selectivity towards ethylene, while other studies showed that Pd primarily promotes the production of ethane. A fundamental understanding of achieving high selectivity is still very limited. Currently, bimetallic systems such as Pd–Ag,[24,25] Pd–Zn,[26] and Pd–Au (ref. 27) have been synthesized and used to improve the selectivity of acetylene hydrogenation. A recent study showed that Pd nanoclusters confined within sodalite (SOD) zeolite (Pd@SOD) exhibit an improved selectivity to ethylene.[28] This divergent performance of Pd-based catalysts suggests that there is still significant room for improved understanding of the fundamental factors that control the activity and selectivity of acetylene hydrogenation.

In this work, we hypothesize that the activity and selectivity of pure Pd catalysts are highly structure dependent.

School of Chemistry and Chemical Engineering, Queen's University Belfast, David Keir Building, Stranmillis Road, Belfast, BT9 5AG, UK. E-mail: p.hu@qub.ac.uk

† Electronic supplementary information (ESI) available. See DOI: 10.1039/d1cy00665g

5212 | *Catal. Sci. Technol.*, 2021, **11**, 5212–5222

This journal is © The Royal Society of Chemistry 2021

The recently developed microkinetic modelling using energies from density functional theory (DFT) calculations has emerged as a powerful tool for understanding heterogeneous catalysis.[10,29–35] It provides the respective rates of the different reaction pathways, thus allowing the selectivity to the various products to be distinguished by quantitative means.[29] It now has the potential to interpret the contradictions among a variety of studies in the literature from a theoretical point of view and to verify the hypothesis by calculations. In our previous work, we carried out a detailed microkinetic analysis of selective acetylene hydrogenation reaction on the flat Pd(111) surface. Taking the coverage effect into account and using methods such as *ab initio* molecular dynamics (AIMD) to obtain energetic details that are not readily available in traditional calculations bring new insights to the reaction kinetics.[29,36,37] This framework has included self and cross adsorbate–adsorbate interactions, in order to provide a quantitative description of differential chemisorption energies on different structured surfaces. The microkinetic model achieves agreement with experimental results on Pd(111) and lays the foundation for our study of structural sensitivity. The structure sensitivity of Pd catalysts has been suggested previously,[5,38] but it has not been described quantitatively. Furthermore, the activity and selectivity were found to change during reaction with the particle size.[3] The smaller the sizes of particles are, the more defects it is expected for them to have on the surfaces.[39] In an effort to provide a solid theoretical understanding of the structure effect on selectivity and activity, a detailed study of selective acetylene hydrogenation on a Pd surface with defects is highly desirable. In this work, we aim to answer the following questions. (i) How different is the activity and selectivity on the Pd(211) surface compared to Pd(111)? (ii) How are the activity and selectivity on the stepped Pd(211) surface affected by the coverage effects? (iii) What kind of quantitative understanding can we obtain by means of kinetic analysis?

Herein, acetylene hydrogenation is studied on the Pd(211) surface using DFT calculations and coverage-dependent microkinetic simulations. Firstly, a coverage-independent model, as a reference, was built to investigate the acetylene hydrogenation reactions on the stepped Pd surface. The reaction pathways were thoroughly mapped out and compared with reaction pathways on Pd(111). Based on the coverage-independent results, C_2H_2 and H were chosen as the environmental species to calculate the coverage-dependent differential chemisorption energies. Both self and cross adsorbate–adsorbate interactions *versus* the environmental species were thoroughly studied. The transition state energies were corrected with the coverage effect as well. To achieve more accurate kinetic results, the ethylene desorption energy barrier was obtained using the AIMD method based on the steady-state results obtained from coverage-dependent calculations.[37] Ethylene activity and selectivity were explicitly investigated using microkinetic

simulations on Pd(211). Our simulations find the Pd(211) surface to be much more active than the Pd(111) surface, while a strong differential chemisorption energy and lower further hydrogenation barrier of ethylene limit the selectivity. Our results indicate that close-packed surfaces are responsible for the ethylene production over Pd catalysts, while defect sites are significantly more active but selective toward ethane. Furthermore, a sensitivity analysis was carried out to quantitatively assess which physical quantity has a larger influence on ethylene selectivity on Pd(211), thus providing new insights into how surface defects impact on the selectivity. Notably, the catalytic hydrogenation of acetylene over Pd catalysts is highly intricate, and alterations in the Pd metal structure such as hydride and carbide formation can directly influence the reaction kinetics.[11,40,41] In this work, we focus solely on the ideal Pd surfaces.

Computational method

Computational details

In this work, all the DFT energies were calculated using the Vienna *ab initio* simulation package (VASP)[42,43] under the framework of the generalized gradient approximation (GGA) with the Perdew–Burke–Ernzerhof (PBE) functional.[44] The projector-augmented-wave (PAW) pseudopotentials were used,[43,45] and the cutoff energy of plane-wave basis expansion was set to 400 eV. All the gas-phase molecules, including H_2, C_2H_2, C_2H_4, and C_2H_6, were placed in a (10 × 10 × 10) Å^3 cubic box to obtain the total energies. The transition states (TS) were searched using the constrained minimization technique and the quasi-Newton algorithm.[46–49] The transition states were verified by two key facts: (i) all forces on atoms have been optimized to be less than 0.05 eV/Å; (ii) the total energy is a maximum along the reaction coordinate but a minimum with respect to all other degrees of freedom.

Ab initio molecular dynamics was used to investigate the desorption barrier of ethylene in this work using the VASP code, including constrained MD and umbrella sampling.[50,51] The *k*-point 2 × 2 × 1 was used. The time step was 1.0 fs. The Nosé–Hoover[52] thermostat was used to control the temperature, and the free energy is the Helmholtz free energy corresponding to the NVT ensemble.[53] All energies used in this work were free energies. Vibrational frequency analyses were used to correct free energy from the total energy among initial states, transition states, and final states. The thermodynamic corrections of the gaseous species were calculated using Gaussian 03 with ideal gas approximation (only the correction values were used).

Microkinetic model with a coverage effect

A coverage-dependent microkinetic model was used to thoroughly study the acetylene hydrogenation on the Pd(211) surface. 7 elementary steps listed in Table 1 were considered in this work.[5] r_i is the rate of reaction for step i, where $i = 1$, ···7. k_i and k_{-i} are the forward rate and reverse rate constants,

This journal is © The Royal Society of Chemistry 2021

Catal. Sci. Technol., 2021, **11**, 5212–5222 | **5213**

Table 1 Elementary steps and the rate equations of acetylene hydrogenation used in the microkinetic modelling (* represents one free site on the surface, and all C_2H_x species are considered occupying 2 free sites)

	Surface reactions	Rate equations
1	$C_2H_2(g) + 2* \leftrightarrow C_2H_2^*$	$r_1 = k_1 P_{C_2H_2} \theta_*^2 - k_{-1} \theta_{C_2H_2}$
2	$H_2(g) + 2* \leftrightarrow 2H^*$	$r_2 = k_2 P_{H_2} \theta_*^2 - k_{-2} \theta_H^2$
3	$C_2H_2^* + H^* \leftrightarrow C_2H_3^* + *$	$r_3 = k_3 \theta_{C_2H_2} \theta_H - k_{-3} \theta_{C_2H_3} \theta_*$
4	$C_2H_3^* + H^* \leftrightarrow C_2H_4^* + *$	$r_4 = k_4 \theta_{C_2H_3} \theta_H - k_{-4} \theta_{C_2H_4} \theta_*$
5	$C_2H_4^* \leftrightarrow C_2H(g) + 2*$	$r_5 = k_5 \theta_{C_2H_4} - k_{-5} P_{C_2H_4} \theta_*^2$
6	$C_2H_4^* + H^* \leftrightarrow C_2H_5^* + *$	$r_6 = k_6 \theta_{C_2H_4} \theta_H - k_{-6} \theta_{C_2H_5} \theta_*$
7	$C_2H_5^* + H^* \leftrightarrow C_2H_6(g) + 3*$	$r_7 = k_7 \theta_{C_2H_5} \theta_H - k_{-7} P_{C_2H_6} \theta_*^3$

respectively. The transition state theory was used to calculate the rate constants as

$$k_i = \frac{k_B T}{h} e^{-\Delta G_i^{\ddagger}/k_B T}$$

where k_B is the Boltzmann constant, T is the temperature, h is Planck's constant, and $\Delta G_i^{\ddagger}$ is the change of standard free energies between the transition state and the initial state for step i from the DFT calculations.

The differential chemisorption free energy of all species under different coverage conditions is defined as

$$G_{ads(i)}^{diff}(\theta_N) = G_{ads,N} - G_{env,N-1} - G_{gas}$$

where $G_{ads,N}$ and $G_{env,N-1}$ are the free energy after adsorption N adsorbates and the $N-1$ environment species, respectively, and G_{gas} is the free energy of the adsorbate in the gas phase.

We introduced a two-line model to quantify how the coverage effect prevails in the chemisorption energies and reaction barriers.[30,36] The two-line model illustrates how the differential chemisorption energy changes at both low and high coverages. The two-line model describes the linear nature of the differential chemisorption free energy[54,55]–coverage relation. The influence of adsorbate–adsorbate interactions at different coverages with multiple species on differential chemisorption free energy can be written as:

$$G_{ads(i)}^{diff}(\theta) = \begin{cases} \sum_j \left(a_{i/j} \times \theta_j \right) + \sum_j \left(b_{i/j} \times \frac{\theta_j}{\theta} \right) & \theta \leq \theta_c \\ \sum_j \left(a'_{i/j} \times \theta_j \right) + \sum_j \left(b'_{i/j} \times \frac{\theta_j}{\theta} \right) & \theta > \theta_c \end{cases}$$

where θ, θ_j, i and j represent the total coverage, the coverage of species j, the target adsorbate, and the environmental species, respectively. a and b are the slope and intercept of the two-line model; a and b are used to define the linear relationship in the low coverage region, while a' and b' are for the high coverage region. $a_{i/j}$ is a measure of degree to which the coverage of environmental species j affects the

differential chemisorption energy of target adsorbate i if the coverage of j is increased. θ_c is the critical point separating the low coverage from the high coverage.

The turnover frequency (TOF) was calculated using a self-consistent microkinetic model shown in Fig. S10.†[14,56] The microkinetic modelling and analysis were performed using CATKINAS.[57–59] The converged TOF and coverages for different species at the steady state were achieved when the convergence of coverages reaches the level that is smaller enough.

Results and discussion

Coverage-independent model on Pd(211)

The acetylene hydrogenation reactions on Pd(211) was first studied using a traditional coverage-independent model in order to take a glimpse of the reaction kinetics and to provide clues for the selection of major adsorbates, referred to as environmental species (env) in the following sections of coverage-dependent studies. Prior to investigating each elementary step of acetylene hydrogenation, it is necessary first to understand the adsorption of relevant species on Pd(211). Table 2 lists the adsorption energies at 300 K for C_2H_2 and C_2H_4 on Pd(211) compared to those on Pd(111), while Fig. 1 illustrates the preferred adsorption geometries for all C_2H_x on Pd(211).

The favorable adsorption geometry of C_2H_2 is on the B5 site under the step edge, and C_2H_4 is found to adsorb on the step edge with a di-σ configuration, which is consistent with previously reported results.[5,60] For C_2H_2, the adsorption energy of −2.33 eV on Pd(211) suggests a strong chemisorption, and the binding energy is slightly larger than that on Pd(111), which has an adsorption energy of −2.01 eV. However, the free adsorption energies of C_2H_2 on both Pd(211) and Pd(111) become relatively close with a small difference of 0.13 eV at 300 K. For C_2H_4, the adsorption energy of −1.21 eV on Pd(211) is larger than that on Pd(111) (−0.87 eV). In contrast to C_2H_2, when the temperature is considered, there is still a significant gap of 0.52 eV between the free adsorption energies of C_2H_4 on Pd(111) and Pd(211). The energy difference suggests that C_2H_4 binds much stronger onto Pd(211) than Pd(111). To further study the acetylene hydrogenation on the stepped Pd surface, the reaction energies and reaction barriers for all elementary steps were calculated. The results and transition state geometries are shown in Fig. 2.

Table 2 Adsorption energies (E_{ads}/eV) and free adsorption energies (G_{ads}/eV) of C_2H_2 and C_2H_4 on Pd(211) and Pd(111). The results on Pd(111) were taken from our previous work[37]

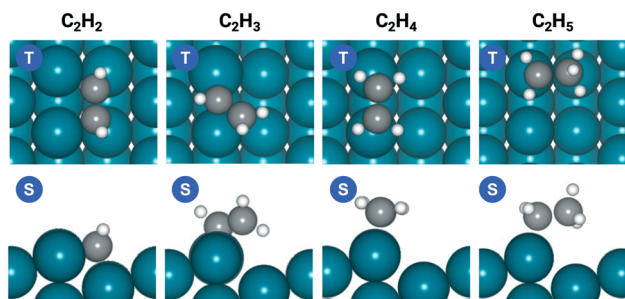|	Pd(211)		Pd(111)	
	E_{ads}	G_{ads}	E_{ads}	G_{ads}
C_2H_2	−2.33	−1.65	−2.01	−1.49
C_2H_4	−1.21	−0.81	−0.87	−0.34

Fig. 1 Top (T) and side (S) views of C_2H_2, C_2H_3, C_2H_4, and C_2H_5 adsorption geometries on Pd(211).

The reaction barriers for hydrogenation reactions of C_2H_2, C_2H_3, C_2H_4, and C_2H_5 on Pd(211) were calculated to be 0.75 eV, 0.38 eV, 0.63 eV and 0.53 eV, respectively. The following observations are worth noting. (i) For the first and last hydrogenation steps, the barriers obtained on Pd(111) and Pd(211) are almost identical. However, the hydrogenation barriers of C_2H_3 and C_2H_4 are significantly reduced on Pd(211). (ii) The rate-determining step is found to be the first hydrogenation step, without considering the coverage effect, as in the reaction on Pd(111).

Recalling our previous coverage-dependent study on Pd(111),[37] the reason for choosing both C_2H_2 and C_2H_3 as environmental species was that the C_2H_3 hydrogenation is kinetically hindered and the barrier is as high as that of the first hydrogenation step, which is the rate-limiting step on Pd(111). With the C_2H_3 hydrogenation barrier dropped significantly on Pd(211), the conversion rate of C_2H_3 become much faster than that that on Pd(111), resulting in far less C_2H_3 on the Pd(211) surface. Therefore, only C_2H_2 and H are
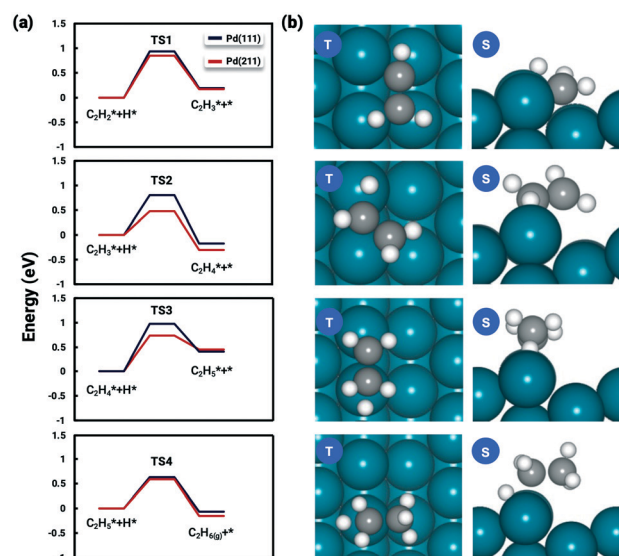
selected as the environmental species for the coverage-dependent study. The lowered barriers should potentially impact the selectivity and activity of acetylene hydrogenation on Pd(211). We will discuss reaction kinetics in later sections.

Coverage-dependent model on Pd(211)

With insights from the coverage-independent model, two major adsorbates, H atom and C_2H_2 molecule, were selected as the environmental species, which pre-occupied the surface, to conduct the coverage-dependent kinetic modelling. The concept of differential chemisorption energy from the method section was applied to investigate both self and cross-interactions between different adsorbates *versus* the environmental species. The transition state energies were also rigorously calculated to add more details to the coverage-dependent microkinetic model. In general, for each coverage, all of the possible configurations are calculated, and the structure with the lowest energy is selected to obtain the differential chemisorption energy.

The coverage effect caused by C_2H_2 as the environmental species was firstly determined, taking into account both self and cross interactions. In pursuit of higher accuracy, how to determine the accurate coverage of the surface adsorbates needs to be carefully studied; different adsorption structures on the Pd(211) surface can lead to variations in the number of sites occupied by adsorbates. For C_2H_2, if it adsorbs on the B5 and hcp sites, then it occupies 2 sites in the calculation of the differential chemisorption energy. The differential chemisorption energies with the adsorbate–adsorbate interactions were obtained using six different coverages to establish the two-line model. Taking the self-interaction of C_2H_2 as an example, the optimized structures of C_2H_2 adsorbed on the Pd(211) surface are illustrated in Fig. 3.

Fig. 2 (a) Comparison of energy profiles of the hydrogenation of C_2H_2, C_2H_3, C_2H_4, and C_2H_5 on Pd(211) and Pd(111). * indicates the adsorption states. TS1, TS2, TS3, and TS4 are the transition states of the hydrogenation steps. (b) Top and side views of transition state geometries on Pd(211).
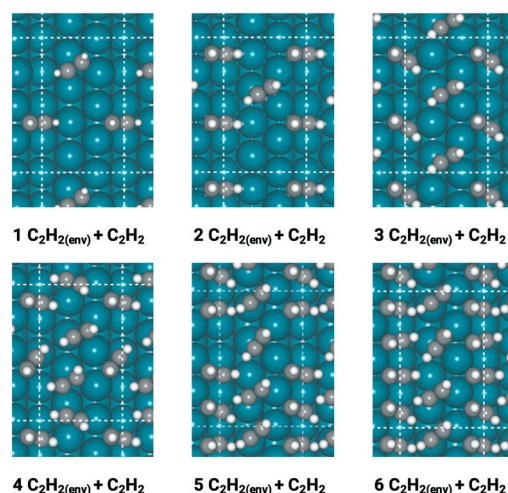

Fig. 3 Most stable structures of $C_2H_2^*/C_2H_{2(env)}$ on the stepped Pd(211) surface. The white, grey, and dark blue atoms represent H, C, and Pd, respectively. After determining the adsorption sites for each C_2H_2, the corresponding coverages were determined to be 0.250 ML, 0.417 ML, 0.500 ML, 0.583 ML, 0.667 ML, and 0.833 ML, respectively.

The differential chemisorption energies of all C_2H_x species on the C_2H_2 pre-occupied surface were then calculated, and results are shown in Fig. 4. Fig. 4(a) shows the self-interaction of $C_2H_2^*/C_2H_{2(env)}$; when increasing the number of existing surface adsorbates, the differential chemisorption energy of the incoming molecule is weakened. This result can be simply explained by the Pauli repulsion effect and the bonding competition.[61–63] When one adsorbate binds to a surface, the surface becomes inert and hinders further binding to a second adsorbate, resulting in a decrease of chemisorption energy. Therefore, the more existing adsorbates the surface possesses, the weaker the chemisorption energy becomes.

Likewise, the coverage effect caused by hydrogen atoms was rigorously studied on the Pd(211) surface (Fig. 5). Interestingly, the affected differential chemisorption energy displaces an almost uniform increasing trend, which differs from the results obtained on the Pd(111) surface, and does not show a particularly clear coverage to be distinguished between high and low coverages. This may be due to two reasons. (i) In a previous study we found that the distinction between high and low coverage is due to the sudden change in the degree to which differential chemisorption energy is affected by coverage which can also be seen from the change in the slope in the two-line model. The slopes in the low coverage region are mainly determined by the adsorbate or the transition state structure, while in the high coverage region the bonding competition with neighboring species becomes the dominant factor. However, on Pd(211), most of the adsorbates are adsorbed on the edge, and it is difficult for the environmental hydrogen atoms that adsorbed on the step side to be truly "neighboring". This results in rather uniform changes in the coverage effect generated by H atoms. (ii) H atom is comparatively smaller, and the resulting repulsive force is more moderate. Therefore, the coverage effect caused
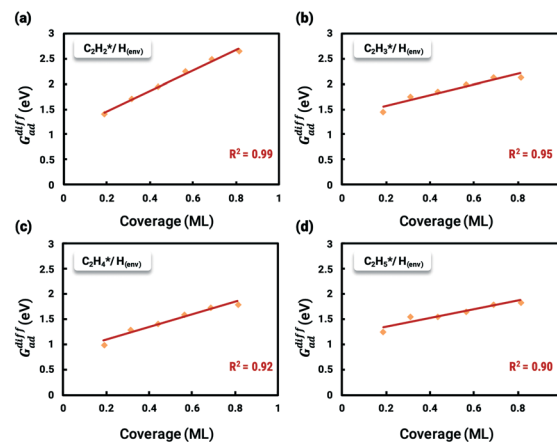

Fig. 5 Relationships between differential chemisorption energies and coverages of cross-interactions. (a) $C_2H_2^*/H_{(env)}$, (b) $C_2H_3^*/H_{(env)}$, (c) $C_2H_4^*/H_{(env)}$, and (d) $C_2H_5^*/H_{(env)}$. The free energies were calculated at a temperature of 300 K.

by H atoms is described using a simplified one-line model. The self-interaction of the H atom on the stepped Pd(211) surface is found to be similar to that on Pd(111), which makes it negligible unless a very high coverage is achieved.[37]

In this work, a total of 8 possible cross-interactions are listed in Table 3. The three trends worth mentioning here are as follows. (i) Among all the adsorbate–adsorbate interactions, the differential chemisorption energy of C_2H_2 was most affected by the self-interaction of C_2H_2 with a slope of 2.47 in the low coverage region and 6.502 in the high coverage region. Such a high influence is mainly due to the adsorption geometry, as shown in Fig. 1. C_2H_2 adsorbs on the B5 site under the step edge; the stepped surface makes it closer to the pre-occupied molecules on the stepped surface, causing an increase of the intermolecular repulsion. In contrast, all other species adsorb on the edge of the stepped Pd(211) surface, making them relatively far away from the environmental molecules, resulting in less intermolecular repulsion. The geometry of adsorption is also responsible for the fact that C_2H_2 is exposed to the coverage effect of H atoms more than other C_2H_x species. (ii) The differential chemisorption energy of the H atom was mostly affected by the coverage of C_2H_2 with a slope of 1.121. (iii) In contrast to the previous work, the overall coverage effect on the stepped
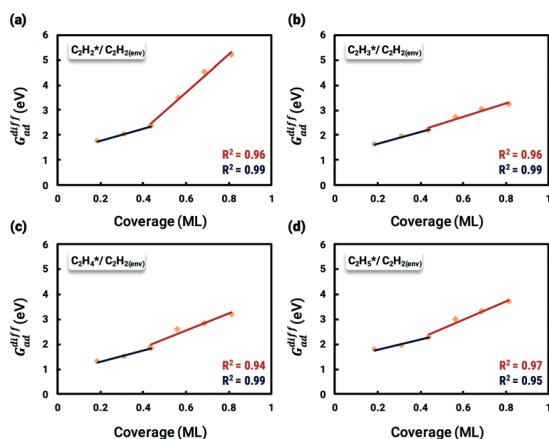

Fig. 4 Relationships between differential chemisorption energies and coverages of cross-interactions. (a) $C_2H_2^*/C_2H_{2(env)}$, (b) $C_2H_3^*/C_2H_{2(env)}$, (c) $C_2H_4^*/C_2H_{2(env)}$, and (d) $C_2H_5^*/C_2H_{2(env)}$. The free energies were calculated at a temperature of 300 K. The black line represents the trend under the low coverage range, and the red line represents the trend under the high coverage range.

Table 3 List of all self- and cross-interactions in the adsorption states for acetylene hydrogenation on Pd(211) with C_2H_2 (two-line model) and H (one-line model) as the environment species individually in each case. The slopes of the interaction curves are also listed

C_2H_2 (env)	Slope		H (env)	Slope
	Low coverage	High coverage		
$C_2H_2^*$	2.47	6.502	$C_2H_2^*$	1.121
$C_2H_3^*$	1.587	2.450	$C_2H_3^*$	0.953
$C_2H_4^*$	1.273	2.382	$C_2H_4^*$	0.976
$C_2H_5^*$	1.344	3.283	$C_2H_5^*$	0.917
H*	0.369	1.335	H*	0.057

surface may not be as dominant as on the flat surface due to the presence of edge sites.[37]

As previously studied in our group, the coverage effects would also significantly affect the reaction barriers.[30,36,37] Transition state energies, as another critical factor, were also explicitly calculated with coverage effects. The structures of the TS–adsorbate interactions are reported in the Fig. S4–S7.† After a thorough study of the transition states at different coverages by the same method previously used for differential chemisorption energy calculations, the energies of the transition states corrected for the coverage effect are found to have a similar trend to that of the differential chemisorption energy: as the total coverage increases, the energies of the transition states become weaker. All the slopes of the interaction between the transition state and environmental species are listed in Table 4.

As seen in Table 4, the energy of the first transition state is mostly affected by the coverage effect caused by C_2H_2 with a slope of 6.640 in the high coverage region and a slope of 2.876 in the low coverage region. This can be rationalized by the adsorption structure of C_2H_2–H*, where it adsorbs on the B5 site at the step edge as shown in Fig. 3, leading to a strong repulsion caused by the other C_2H_2 molecules adsorbed on the step side of the Pd(211) surface. Other transition states primely adsorb on the edge, which makes them less vulnerable to the coverage effect. The reaction barrier of $C_2H_4^* + H^* \leftrightarrow C_2H_5^* + *$ is least affected by the coverage effect caused by C_2H_2 with a slope of 1.891 in the high coverage region and a slope of 1.284 in the low coverage region. The transition state geometry of C_2H_4–H* is nearly perpendicular to the bridge site of the Pd(211) edge, as can be seen in Fig. 3, which isolates it from other adsorbates. Comparing the coverage effects caused by C_2H_2 and H, it is clear that the contribution of C_2H_2 is more significant than that of H, which can be reasonably explained by the stronger differential chemisorption energy of C_2H_2 than that of H and also the greater number of atoms in C_2H_2. It is obvious when comparing the results with those on the Pd(111) surface, except for C_2H_2–H*, that the coverage effect on all other transition states is much smaller on Pd(211) than that on Pd(111).[37]

AIMD determination of the desorption barrier of ethylene on Pd(211)

The key to resolve the underlying question of ethylene selectivity can be summarized as a contrast between the reaction barriers of the desorption process and the hydrogenation reaction of ethylene.[10,37] The coverage-dependent model resolves how pre-occupied molecules influence the transition state energies and can be used to obtain the coverage-dependent barrier of C_2H_4 hydrogenation. The desorption free energy barrier of C_2H_4 was then calculated using the AIMD.[64,65] According to our previous work,[37] we can first set the desorption barrier of ethylene using the traditional method, and then apply the self-consistent calculation mentioned in the method section to obtain the surface coverage for the AIMD simulation. The self-consistent reaction kinetics were calculated using the coverage-effect corrected differential chemisorption energies and reaction barriers discussed in the previous sections. The surface coverages were found to be 0.84 ML at a temperature of 300 K and 0.54 ML at a temperature of 500 K.

Ethylene desorption was calculated using the coordinate of the distance between one of the C atoms and the adsorbed site on the Pd surface from 2.0 Å to 3.5 Å, and a series of biased MD simulations were performed with a distance increment of 0.1 Å. An umbrella sampling with the weighted histogram analysis method (WHAM) was conducted for the ethylene desorption process on Pd(211). The 2d-WHAM code of Grossfield[66] was used with the VASP code, and the Gaussian peak model was chosen for constraints.[67] In Fig. 6, the lowest points of the two curves represent the most stable adsorbed states of C_2H_4 on the pre-occupied stepped Pd(211) surface at 300 and 500 K, respectively, and the peaks of the curves indicate the transition states in the process. The umbrella sampling method gives an ethylene desorption barrier of 0.57 eV at 300 K (Fig. 6a) and 0.43 eV at 500 K (Fig. 6b). Notably, as the desorption barrier is the key energy affecting the selectivity of this reaction system, our AIMD was stopped after the transition states were achieved to save simulation time.

Comparison of the reaction kinetics between the coverage-dependent and coverage-independent methods at 300 K

The coverage-dependent reaction kinetics of acetylene hydrogenation on the Pd(211) surface was investigated using
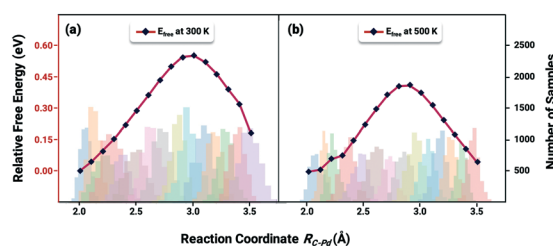
Table 4 List of all cross-interactions between the transition states and adsorbates for acetylene hydrogenation. C_2H_2–H* represents the transition state of C_2H_2 hydrogenation on the surface. The slopes of interaction curves are also listed

Slope				
C_2H_2 (env)	Low coverage	High coverage	H (env)	Slope
C_2H_2–H*	2.876	6.640	C_2H_2–H*	1.837
C_2H_3–H*	3.344	2.613	C_2H_3–H*	1.604
C_2H_4–H*	1.284	1.891	C_2H_4–H*	1.232
C_2H_5–H*	1.304	2.948	C_2H_5–H*	1.327

Fig. 6 Free energy analysis of ethylene desorption from Pd(211) along $R_{C–Pd}$ by umbrella sampling under the following conditions: (a) a surface coverage of 0.84 ML and a temperature of 300 K and (b) a surface coverage of 0.54 ML and a temperature of 500 K. The stacked colour bars are an indication of a complete sampling process, with each bar representing the number of samples collected at that reaction coordinate during the AIMD.

This journal is © The Royal Society of Chemistry 2021

Catal. Sci. Technol., 2021, **11**, 5212–5222 | **5217**

Paper

the microkinetic method based on the energies obtained from coverage-dependent DFT calculations, and thermodynamic corrections were applied to obtain the free energy changes. The ethylene desorption barrier achieved using AIMD was added to the coverage-dependent model in order to make the kinetic calculations more exhaustive. The coverage-independent model was obtained using coverage-independent energies. Both models were conducted under the experimental conditions of 300 K temperature and 100 Torr pressure for both C_2H_2 and H_2. Fig. 7 shows the free energy profiles, the surface distribution obtained from both the coverage-dependent and coverage-independent models and the calculated TOFs.

Several interesting findings emerged when comparing the results from the coverage-dependent and coverage-independent methods (Fig. 7a). (i) Under high coverage conditions, the reaction barriers are reduced and become more processable due to the coverage effect affecting the transition state energies. This finding is consistent with previous studies.[37,68] (ii) After considering the coverage effect, the rate-determining step remains to be the C_2H_2 hydrogenation, unlike the case on Pd(111) in which the coverage effect does decisively change the reaction rate-determining step.[37] The surface coverage distribution was calculated using the self-consistent microkinetic method from the coverage-dependent model after adding the AIMD results. In the coverage-independent model (Fig. 7b), the surface was almost covered completely, being dominantly covered by C_2H_2 due to its more potent differential

chemisorption energy. By factoring in the coverage effect, the differential chemisorption energy of C_2H_2 was drastically reduced, and the surface coverage calculated at the steady-state is 0.84 ML containing 0.56 ML of C_2H_2 and 0.28 ML of H, which is a much reasonable result. The over-estimated differential chemisorption energy of C_2H_2 results in a calculated ethylene TOF of 6.32×10^{-11} s^{-1} (ln(TOF) = −11.07) (Fig. 7c). After obtaining the self and cross adsorbate–adsorbate interactions of each main species and the relationship between adsorbate and transition state, the TOF for the coverage-dependent model was calculated to be 3.9 s^{-1} (ln(TOF) = 1.37), which is closer to the experimental result.[14]

Kinetic analysis of activity and selectivity to ethylene on Pd(211)

The coverage-dependent microkinetic model was then used to further investigate C_2H_4 activity and selectivity on the stepped Pd(211) surface by taking the desorption barrier of ethylene into account. The kinetic simulations performed using the coverage-dependent microkinetic model were set in an acetylene–hydrogen mixture at temperatures of 300 K and 500 K and pressures of 100 Torr each. The resulting TOFs and selectivity were compared (Fig. 8) with the previously calculated results on Pd(111) and the experimental data collected by Molero et al.[14,37] The selectivity used in this work is defined as:
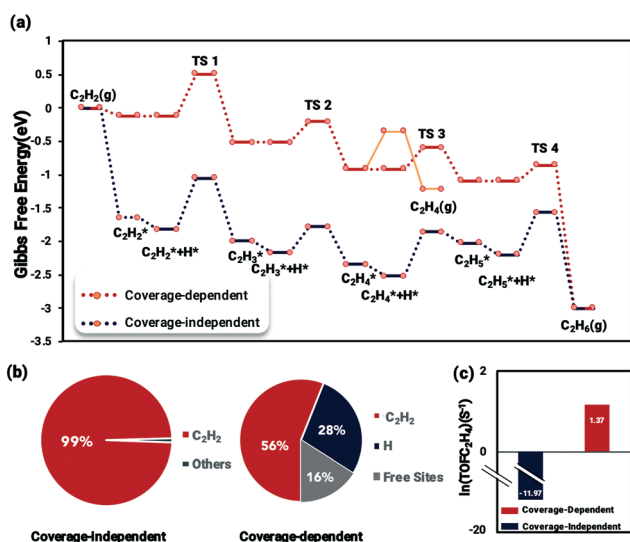

Fig. 7 (a) Comparison of the free energy profiles of coverage-dependent and coverage-independent acetylene hydrogenation on Pd(211) at 300 K; the red line shows coverage-dependent kinetic results, and the black line shows the coverage-independent kinetic results. The orange line shows the ethylene desorption pathway obtained using AIMD. (b) Surface coverage distribution results obtained using the coverage-dependent and coverage-independent methods. (c) TOF values of ethylene formation based on the coverage-independent model (black) and coverage-dependent model (red).
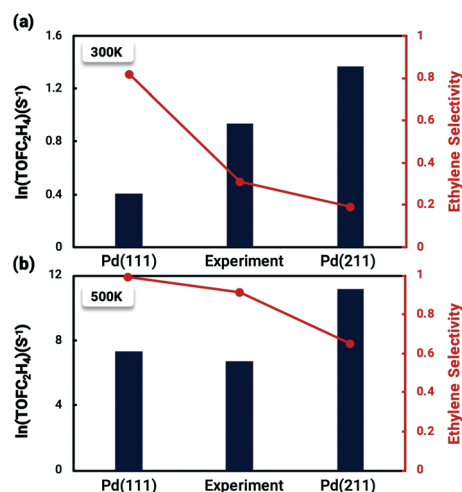

Fig. 8 Comparison between the calculated TOF and selectivity results from the coverage-dependent microkinetic model and the experimental data from Molero et al.[14] of ethylene production from acetylene hydrogenation over Pd(111) and Pd(211) at (a) 300 K and (b) 500 K. The high activity on the Pd(211) surface is primarily due to the decisive role of the coverage effect in reducing the reaction barrier of the rate-determining step, while the poor selectivity is a consequence of the inherently high chemisorption energy of ethylene on the stepped surface. The experimental value lies just in the middle of the two which may indicate that there might be two types of surface sites co-existing on the experimental catalysts. The results on Pd(111) were taken from our previous work.[37]

5218 | Catal. Sci. Technol., 2021, **11**, 5212–5222

This journal is © The Royal Society of Chemistry 2021

$$\text{Selectivity} = \frac{\text{TOF}_{\text{ethylene}}}{\left(\text{TOF}_{\text{ethylene}} + \text{TOF}_{\text{ethane}}\right)}$$

The activity trends of ethylene on Pd(211) and Pd(111) are similar, with a rapid increase in the TOF with increasing temperature. However, the TOFs (Fig. 8) for the stepped Pd(211) surface are much higher than both the experimental data and calculated results on Pd(111) at the investigated temperatures. The TOF of ethylene is as high as 8.74×10^5 s^{-1} (ln(TOF) = 11.3) on Pd(211), while the TOF on Pd(111) is 1.48×10^4 s^{-1} (ln(TOF) = 7.3). The two reasons that might contribute to the larger TOF of Pd(211) than that of Pd(111) are as follows. (i) From the reaction barrier comparison in Fig. 2, in the coverage-independent case the reaction barriers on Pd(211) are already lower than the corresponding barriers on Pd(111). (ii) The coverage effect heavily influences the transition state energies. The slope derived from the two-line model is an indicator of the extent to which the coverage effect affects these energies. As seen in Table 2, the transition state of the rate-determining step is more sharply influenced by the coverage effect on Pd(211) with a slope of 6.604 than that on Pd(111) (slope of 6.085, averaged from the two dominant environmental species: C_2H_2 and C_2H_3).[37] The higher slope leads to the barrier of the rate determining step on Pd(211), which is inherently lower than the barrier on Pd(111), being more affected by the coverage effect. Numerically, the difference between the two barriers is merely about 0.04 eV in the coverage-independent case, but after considering the coverage effect, the barrier of Pd(211) at the steady state is 0.12 eV lower than that of Pd(111) with a similar surface coverage. This gap directly demonstrates that the primary contributor to the high activity on Pd(211) is the dominating influence of the coverage effect on the barrier of the rate-determining step.

The situation is reversed regarding ethylene selectivity. The ethylene selectivity is around 0.2 at 300 K and 0.62 at 500 K on Pd(211), while the selectivity is always above 0.8 on Pd(111). The experimental values from the work of Molero *et al.* are 0.35 at 300 K and 0.87 at 500 K on Pd(111).[14] The agreement between our calculation results and experimental values can be rationalized by the desorption barrier decreasing faster than the hydrogenation barrier of ethylene with increasing temperature. The high selectivity on Pd(111) is reasonable, given that the coverage-dependent microkinetic modelling shows that the free energy barrier for hydrogenating C_2H_4 is higher than the desorption barrier, which favors the desorption process. Since the selectivity is the primary focus of acetylene hydrogenation reactions, it is worthwhile to systematically investigate the reasons for such a low selectivity on Pd(211). The chemisorption energy and reaction barriers of C_2H_4 are chosen as the key aspects to analyze this problem.

Adsorption of C_2H_4. From Table 2, we can see that the adsorption energy of C_2H_4 on Pd(211) is larger than that on Pd(111), indicating robust binding strength. Unlike the case

of C_2H_2, where the coverage effect on the adsorption is significant to obliterate or even reverse the difference in its chemisorption energy under high coverage conditions, the coverage effect on C_2H_4 is far less impactful to make a difference on Pd(211). The slope of the coverage effect of C_2H_4 adsorption on Pd(211) is 2.382, which is much smaller than that of C_2H_4 adsorption on Pd(111), which has a slope of 5.1 (averaged from both two dominant environmental species: C_2H_2 and C_2H_3).[37] The noticeable decrease in the coverage effect is most likely due to the adsorption sites. C_2H_4 adsorbs on the edge site, and by the nature of the stepped Pd(211) surface and its convex shape, the adsorbates on the edge site are relatively isolated from the environmental species adsorbed on other sites, resulting in less repulsion and a steric hindrance between molecules. This implies that C_2H_4 on Pd(211) maintains strong binding strength even at very high coverages, making the desorption process difficult.

Hydrogenation and desorption barriers of C_2H_4. The geometric effect of the Pd(211) surface on the differential chemisorption energy of C_2H_4 can also be found on the transition state energy of C_2H_4–H*. The transition state of C_2H_4–H* is on the edge site, shrinking the impact of the coverage effect with a slope of only 2.382 compared to a slope of 5.951 on Pd(111).[37] As previously discussed, the competition between the desorption and hydrogenation barriers is the key to ethylene formation.[10,37] A relatively small slope value of 1.891 compared to the drastic change (7.829) on Pd(111) means that the energy barrier of this reaction step tends to decrease more moderately when the coverage rises, which in a way facilitates the desorption of ethylene. The AIMD simulations show that the barrier of C_2H_4 desorption on Pd(211) is relatively high at 0.57 eV at 300 K, even with a high coverage, and larger than the barrier obtained on Pd(111) with less coverage. The high desorption barrier becomes a major obstacle preventing ethylene desorption. Even at the coverage as high as 0.85, the desorption barrier is higher than the hydrogenation barrier of C_2H_4 on Pd(211) (Fig. 2), resulting in the hydrogenation reaction being favored over desorption.

With these analyses, it is clear that the issue of the selectivity is different from the activity. Due to the geometrical effect of the Pd(211) surface, which leads to the coverage effect becoming less influential, the poor selectivity on the Pd(211) surface is mainly caused by the inherent and excessive differential chemisorption energy of ethylene. By revealing how geometric effects can influence the role of surface coverage, we have thus demonstrated that different structures of the same catalyst can lead to vastly different activity and selectivity results.

It is worth further identifying which physical quantity has the most significant effect on ethylene selectivity among surface defects. A sensitivity analysis was then performed to test which had a greater effect on selectivity, the desorption barrier of ethylene or the hydrogenation barrier of $C_2H_4^*$. The sensitivity analysis was carried out based on the steady-state
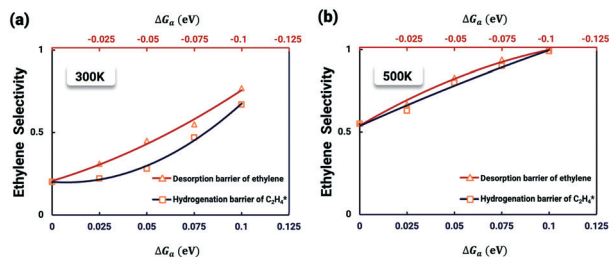
Fig. 9 Sensitivity analysis of ethylene selectivity by nudging the kinetic parameters at (a) 300 K and (b) 500 K. The red curve shows the change of ethylene selectivity as the ethylene desorption barrier is decreased, while the black curve shows the effect of increasing the hydrogenation barrier of $C_2H_4^*$ on the selectivity.

results obtained using the coverage-dependent microkinetic model at 300 and 500 K.[37] The selected parameters are allowed to vary within a narrow range of 0.1 eV, while other factors remain constant during the test. Fig. 9 shows the resulting trends; the black curve shows the change of ethylene selectivity as the hydrogenation barrier of $C_2H_4^*$ is increased, while the red curve shows the effect of decreasing the ethylene desorption barrier on the selectivity. The selectivity to ethylene increases when the desorption barrier drops or the hydrogenation barrier increases. Under low temperature conditions, as shown in Fig. 9a, we find that lowering the desorption barrier is significantly more effective in enhancing ethylene selectivity than increasing the hydrogenation barrier. The ethylene selectivity increases from 0.2 to 0.43 as the desorption barrier of ethylene is decreased by 0.05 eV; with the hydrogenation barrier being increased by 0.05 eV, the selectivity increases only by 10%. When the swing range exceeds 0.1 eV under high temperature conditions as shown in Fig. 9b, a change of either barrier will result in a selectivity higher than 99%. With the above trends, the design of Pd catalysts with reduced ethylene desorption energy barriers can help to significantly improve the selectivity to ethylene on catalysts with possible surface defects.

Conclusions

This work was motivated by two reasons. The first one was to confirm a speculation in our previous work that the difference in ethylene selectivity between the calculated results and the experiment data on Pd(111) was due to the surface defects. The second one, perhaps the more important one, is to truly understand the structural effects on the activity/selectivity of acetylene hydrogenation. Thus, an attempt to quantitatively determine ethylene activity as well as the selectivity of acetylene hydrogenation on the stepped Pd(211) surface using detailed microkinetic simulations that take the coverage effect into account is presented in order to answer how surface defects can influence reaction kinetics. Both pathways to C_2H_4 and C_2H_6 were calculated at relevant surface coverages thus explicitly accounting for all the major

adsorbate–adsorbate interactions. With the thorough comparison between results obtained from Pd(111) and Pd(211), it was found that the selectivity towards C_2H_4 is highly structure-dependent. As a result, through rigorous calculation and kinetic analysis, an in-depth understanding of the reaction kinetics on the stepped surface was developed, and the following conclusions are reached.

A coverage-independent model was first established to map out the reaction landscape of acetylene hydrogenation on the stepped Pd(211) surface. From this model, the hydrogenation barriers of C_2H_3 and C_2H_4 on Pd(211) are significantly reduced compared to Pd(111). Thus, only C_2H_2 and H are chosen as the environmental species for the coverage-dependent study.

The coverage-dependent microkinetic modelling was then performed self-consistently, and the coverage self and cross-interactions of adsorbates were rigorously calculated. It was found interestingly that the coverage effect has a particularly prominent effect on the differential chemisorption energy of C_2H_2 and its transition state energy for hydrogenation reactions compared to other species. This phenomenon is caused by a geometric effect, where Pd(211) has different active sites by its nature, with C_2H_2 adsorbed on the B5 site under the step edge, leading to stronger repulsion of other molecules adsorbed on the step of the Pd(211) surface.

The free energy barriers of the ethylene desorption process on Pd(211) with the surface coverage of steady states were revealed using AIMD. The free energy barriers were found to be at 0.57 eV at 300 K and 0.43 eV at 500 K, higher than the desorption barriers on Pd(111).

A high activity and low selectivity were obtained by the coverage-dependent microkinetic modelling combined with the AIMD. A quantitative analysis was carried out to explore the origin of this result. The high activity on Pd(211) is due to the dominating influence of the coverage effect on lowering the barrier of the rate-determining step. The poor selectivity is a result of the inherent and excessive chemisorption energy of ethylene on the step edge while being less influenced by the coverage effect, leading to a tendency to the further hydrogenation of C_2H_4 rather than the desorption.

A sensitivity analysis was performed to further investigate the ethylene selectivity of the reaction system based on our kinetic model. Similar to the results of Pd(111), both the desorption barrier of ethylene and the hydrogenation barrier of C_2H_4 have impacts on the selectivity to ethylene on Pd(211). Moreover, we found that lowering the desorption barrier gives better results for improving the selectivity at low temperatures.

Real Pd catalysts contain flat surface areas with surface defects, being perhaps best represented by a mixture of Pd(111) and Pd(211) surfaces. This work proposed an atomic level explanation for the differences in catalytic activity and selectivity reported in various literature studies, even for nominally identical catalysts.

5220 | *Catal. Sci. Technol.*, 2021, **11**, 5212–5222

This journal is © The Royal Society of Chemistry 2021

Conflicts of interest

There are no conflicts to declare.

Acknowledgements

References

1 Z. Sun, S. Wang and W. Chen, *J. Mater. Chem. A*, 2021, **9**, 5296–5319.

2 J. F. Chen, Y. Mao, H. F. Wang and P. Hu, *ACS Catal.*, 2019, **9**, 2633–2638.

3 G. Vilé, D. Albani, N. Almora-Barrios, N. López and J. Pérez-Ramírez, *ChemCatChem*, 2016, **8**, 21–33.

4 D. S. Sholl and R. P. Lively, *Nature*, 2016, **532**, 6–9.

5 B. Yang, R. Burch, C. Hardacre, G. Headdock and P. Hu, *J. Catal.*, 2013, **305**, 264–276.

6 A. Borodziński and G. C. Bond, *Catal. Rev.: Sci. Eng.*, 2006, **48**, 91–144.

7 M. Larsson, J. Jansson and S. Asplund, *J. Catal.*, 1998, **178**, 49–57.

8 S. Asplund, *J. Catal.*, 1996, **158**, 267–278.

9 E. Vignola, S. N. Steinmann, A. Al Farra, B. D. Vandegehuchte, D. Curulla and P. Sautet, *ACS Catal.*, 2018, **8**, 1662–1671.

10 F. Studt, F. Abild-Pedersen, T. Bligaard, R. Z. Sorensen, C. H. Christensen and J. K. Norskov, *Science*, 2008, **320**, 1320–1322.

11 F. Studt, F. Abild-Pedersen, T. Bligaard, R. Z. Sørensen, C. H. Christensen and J. K. Nørskov, *Angew. Chem., Int. Ed.*, 2008, **47**, 9299–9302.

12 Y. Cao, H. Zhang, S. Ji, Z. Sui, Z. Jiang, D. Wang, F. Zaera, X. Zhou, X. Duan and Y. Li, *Angew. Chem.*, 2020, **132**, 11744–11749.

13 F. Huang, Y. Deng, Y. Chen, X. Cai, M. Peng, Z. Jia, J. Xie, D. Xiao, X. Wen, N. Wang, Z. Jiang, H. Liu and D. Ma, *Nat. Commun.*, 2019, **10**, 1–7.

14 H. Molero, B. F. Bartlett and W. T. Tysoe, *J. Catal.*, 1999, **181**, 49–56.

15 W. J. Kim, E. W. Shin, J. H. Kang and S. H. Moon, *Appl. Catal., A*, 2003, **251**, 305–313.

16 L. Li, R. B. Lin, R. Krishna, X. Wang, B. Li, H. Wu, J. Li, W. Zhou and B. Chen, *J. Mater. Chem. A*, 2017, **5**, 18984–18988.

17 G. Vilé, D. Albani, M. Nachtegaal, Z. Chen, D. Dontsova, M. Antonietti, N. López and J. Pérez-Ramírez, *Angew. Chem., Int. Ed.*, 2015, **54**, 11265–11269.

18 D. Duca, Z. Varga, G. La Manna and T. Vidóczy, *Theor. Chem. Acc.*, 2000, **104**, 302–311.

19 D. Mei, P. A. Sheth, M. Neurock and C. M. Smith, *J. Catal.*, 2006, **242**, 1–15.

20 M. Jørgensen and H. Grönbeck, *J. Am. Chem. Soc.*, 2019, **141**, 8541–8549.

21 D. Duca, G. Barone and Z. Varga, *Catal. Lett.*, 2001, **72**, 17–23.

22 P. A. Sheth, M. Neurock and C. M. Smith, *J. Phys. Chem. B*, 2003, **107**, 2009–2017.

23 J. Zhao, S. Zha, R. Mu, Z. J. Zhao and J. Gong, *J. Phys. Chem. C*, 2018, **122**, 6005–6013.

24 Y. He, Y. Liu, P. Yang, Y. Du, J. Feng, X. Cao, J. Yang and D. Li, *J. Catal.*, 2015, **330**, 61–70.

25 Y. Liu, J. Zhao, Y. He, J. Feng, T. Wu and D. Li, *J. Catal.*, 2017, **348**, 135–145.

26 H. Zhou, X. Yang, L. Li, X. Liu, Y. Huang, X. Pan, A. Wang, J. Li and T. Zhang, *ACS Catal.*, 2016, **6**, 1054–1061.

27 C. Ma, Y. Du, J. Feng, X. Cao, J. Yang and D. Li, *J. Catal.*, 2014, **317**, 263–271.

28 S. Wang, Z. J. Zhao, X. Chang, J. Zhao, H. Tian, C. Yang, M. Li, Q. Fu, R. Mu and J. Gong, *Angew. Chem., Int. Ed.*, 2019, **58**, 7668–7672.

29 Z. Yao, C. Guo, Y. Mao and P. Hu, *ACS Catal.*, 2019, **9**, 5957–5973.

30 C. Guo, Y. Mao, Z. Yao, J. Chen and P. Hu, *J. Catal.*, 2019, **379**, 52–59.

31 F. Wang, W. Xie, L. Yang, D. Xie and S. Lin, *J. Catal.*, 2021, **396**, 215–223.

32 Y. Mao and P. Hu, *Sci. China: Chem.*, 2020, **63**, 850–859.

33 Z. Wang, H. F. Wang and P. Hu, *Chem. Sci.*, 2015, **6**, 5703–5711.

34 Z. Yao, J. Zhao, R. J. Bunting, C. Zhao, P. Hu and J. Wang, *ACS Catal.*, 2021, 1202–1221.

35 M. Rellán-Piñeiro and N. López, *ACS Sustainable Chem. Eng.*, 2018, **6**, 16169–16178.

36 Y. Ding, Y. Xu, Y. Song, C. Guo and P. Hu, *J. Phys. Chem. C*, 2019, **123**, 27594–27602.

37 W. Xie, J. Xu, Y. Ding and P. Hu, *ACS Catal.*, 2021, 4094–4106.

38 B. Yang, R. Burch, C. Hardacre, P. Hu and P. Hughes, *Catal. Sci. Technol.*, 2017, **7**, 1508–1514.

39 M. Jørgensen and H. Grönbeck, *J. Am. Chem. Soc.*, 2019, **141**, 8541–8549.

40 B. Yang, R. Burch, C. Hardacre, P. Hu and P. Hughes, *Surf. Sci.*, 2016, **646**, 45–49.

41 X.-T. Li, L. Chen, G. Wei, C. Shang and Z.-P. Liu, *ACS Catal.*, 2020, **10**, 9694–9705.

42 G. Kresse and J. Furthmüller, *Phys. Rev. B: Condens. Matter Mater. Phys.*, 1996, **54**, 11169–11186.

43 G. Kresse and D. Joubert, *Phys. Rev. B: Condens. Matter Mater. Phys.*, 1999, **59**, 1758–1775.

44 J. P. Perdew, K. Burke and M. Ernzerhof, *Phys. Rev. Lett.*, 1996, **77**, 3865–3868.

45 P. E. Blöchl, O. Jepsen and O. K. Andersen, *Phys. Rev. B: Condens. Matter Mater. Phys.*, 1994, **49**, 16223–16233.

This journal is © The Royal Society of Chemistry 2021

Catal. Sci. Technol., 2021, **11**, 5212–5222 | **5221**

46 H. F. Wang and Z. P. Liu, *J. Am. Chem. Soc.*, 2008, **130**, 10996–11004.

47 A. Alavi, P. Hu, T. Deutsch, P. L. Silvestrelli and J. Hutter, *Phys. Rev. Lett.*, 1998, **80**, 3650–3653.

48 A. Michaelides, Z. P. Liu, C. J. Zhang, A. Alavi, D. A. King and P. Hu, *J. Am. Chem. Soc.*, 2003, **125**, 3704–3705.

49 Z. P. Liu and P. Hu, *J. Am. Chem. Soc.*, 2003, **125**, 1958–1967.

50 J. Kästner, *Wiley Interdiscip. Rev.: Comput. Mol. Sci.*, 2011, **1**, 932–942.

51 T. Bucko, *J. Phys.: Condens. Matter*, 2008, **20**(6), 064211.

52 H. A. Posch, W. G. Hoover and F. J. Vesely, *Phys. Rev. A: At., Mol., Opt. Phys.*, 1986, **33**, 4253–4265.

53 H. A. Posch, W. G. Hoover and F. J. Vesely, *Phys. Rev. A: At., Mol., Opt. Phys.*, 1986, **33**, 4253–4265.

54 L. C. Grabow, B. Hvolbæk and J. K. Nørskov, *Top. Catal.*, 2010, **53**, 298–310.

55 N. Yang, A. J. Medford, X. Liu, F. Studt, T. Bligaard, S. F. Bent and J. K. Nørskov, *J. Am. Chem. Soc.*, 2016, **138**, 3705–3714.

56 D. Mei, P. A. Sheth, M. Neurock and C. M. Smith, *J. Catal.*, 2006, **242**, 1–15.

57 J. F. Chen, Y. Mao, H. F. Wang and P. Hu, *ACS Catal.*, 2016, **6**, 7078–7087.

58 X. Sun, P. Wang, Z. Shao, X. Cao and P. Hu, *Sci. China: Chem.*, 2019, **62**, 1686–1697.

59 J. Chen, M. Jia, P. Hu and H. Wang, *J. Comput. Chem.*, 2021, **42**, 379–391.

60 J. Andersin and K. Honkala, *Surf. Sci.*, 2010, **604**, 762–769.

61 K. Bleakley and P. Hu, *J. Am. Chem. Soc.*, 1999, **121**, 7644–7652.

62 P. J. Feibelman, *Phys. Rev. B: Condens. Matter Mater. Phys.*, 1988, **38**, 12133–12138.

63 Z. P. Liu, P. Hu and M. H. Lee, *J. Chem. Phys.*, 2003, **119**, 6282–6289.

64 J. Xu, H. Huang and P. Hu, *Phys. Chem. Chem. Phys.*, 2020, **22**, 21340–21349.

65 C. Guo, Z. Wang, D. Wang, H. F. Wang and P. Hu, *J. Phys. Chem. C*, 2018, **122**, 21478–21483.

66 A. Grossfield, *WHAM: the weighted histogram analysis method, version 2.0.9.*

67 M. Iannuzzi, A. Laio and M. Parrinello, *Phys. Rev. Lett.*, 2003, **90**, 4.

68 D. Mei, M. Neurock and C. M. Smith, *J. Catal.*, 2009, **268**, 181–195.

5222 | *Catal. Sci. Technol.*, 2021, **11**, 5212–5222

This journal is © The Royal Society of Chemistry 2021